PAPER

Check for updates

Spray coating polymer substrates from a green solvent to enhance desalination performances of thin film composites†

Shiliang Lin, [a] Shanshan He, [b] Sulaiman Sarwar, [a] Roxana A. Milescu, [c] Con R. McElroy, [c] Simone Dimartino, [a] Lu Shao [b] and Cher Hon Lau *[a]

Toxic solvents like *n,n*-dimethylformamide (DMF), *n,n*-dimethylethanamide (DMAc), and 1-methyl-2-pyrrolidone (NMP) are commonly used to fabricate polymer support membranes. Replacing these toxic solvents with green solvents such as Cyrene™ can imbue sustainability into membrane fabrication, but at the expense of poor membrane separation performances. Here we overcome this limitation by spray coating Cyrene™-based polymer dope solutions to form highly porous asymmetric membranes. The pure water permeance of spray-coated polyethersulfone (PES) membranes reached 68.9 L m^{-2} h^{-1} bar^{-1}, 7-fold higher than knife cast membranes. This significant increase in permeance was ascribed to a porous, thin skin layer and macrovoids interconnected with finger-like pores in spray-coated PES films. However, this did not impact on the ability to yield thin film composites (TFCs) with high separation performances. Through interfacial polymerisation, we deposited a polyamide selective layer on to the surface of spray-coated PES films to yield TFCs for desalination of a 2000 ppm NaCl solution. The salt rejection rate and permeance of such TFCs reached 93% and 1.76 L m^{-2} h^{-1} bar^{-1}, respectively. This desalination performance was similar to knife cast membranes produced from DMF-, NMP- and DMAc-based polymer dope solutions, but fabricated here in a more sustainable manner. This indicated that spray coating can overcome the trade-off between poor membrane separation performance and sustainability.

Introduction

Ascribing to high separation efficiency,[1] low carbon emission, low energy consumption[2] and simple operation,[3] polymer membrane separations are widely used in industry for water treatment. These include applications in microfiltration (MF), ultrafiltration (UF), nanofiltration (NF), wastewater recycling and desalination.[4–6] Each of these applications require different membranes fabricated from a range of polymers. For example, polyethersulfone (PES) membranes are commonly deployed in applications that require excellent chemical, mechanical and thermal stability.[7–9]

Polymer membranes, including those from PES, are typically fabricated using phase inversion processes such as non-solvent induced phase separation (NIPS),[10] vapor induced phase separation (VIPS)[11] and thermal induced phase separation (TIPS).[12] Amongst these techniques, NIPS is widely used as it is easy to achieve with minimal equipment requirements. NIPS requires a polymer dope solution deposited evenly across a surface, followed by immersion in a non-solvent coagulation bath. This triggers a phase separation process as the working solvent and non-solvent come into contact and are exchanged. This leads to demixing and the formation of a sandwich film structure. The top (skin) layer of this film is formed immediately during solvent exchange at the interface between the dope solution and the non-solvent in the coagulation bath. The middle layer of this film comprises finger-like structures and/or macro voids and the bottom layer is highly porous.[10,13]

The thickness and porosity of the skin layer are critical features that impact membrane permeability.[14] Instantaneous demixing leads to a thin and porous skin layer while delayed demixing creates a thick and dense skin layer.[14,15] Porosity in the skin layer enhances membrane permeability and can be generated by controlling the demixing rate and adding pore forming agents into the dope solution. For example, PES membranes cast from water-miscible solvents such as NMP usually possess thinner skin layers,[14] while highly viscous dope solutions suppress the formation of pores and macrovoids.[16,17]

[a]*School of Engineering, University of Edinburgh, Robert Stevenson Road, EH9 3FK, UK. E-mail: cherhon.lau@ed.ac.uk*

[b]*MIIT Key Laboratory of Critical Materials Technology for New Energy Conversion and Storage, State Key Laboratory of Urban Water Resource and Environment, School of Chemistry and Chemical Engineering, Harbin Institute of Technology, Harbin 150001, P. R. China*

[c]*Department of Chemistry, Green Chemistry Centre of Excellence, University of York, Heslington, York YO10 5DD, UK*

This journal is © The Royal Society of Chemistry 2023

J. Mater. Chem. A, 2023, **11**, 891–900 | 891

Other methods to control demixing include varying coagulation bath composition[18,19] and temperature,[20] controlling the casting speed,[14] and adding porogens into the dope solution. For example, adding water into the dope solution leads to the formation of larger pores and more porous membranes with water permeances that are 150% higher than those of membranes prepared from dehydrated dope solutions.[21] Other pore forming agents include polymers such as polyvinylpyrrolidone (PVP) and polyethylene glycol (PEG). Low molecular weight porogens can also increase overall membrane porosity to enhance pure water fluxes,[22,23] while high molecular weight polymeric pore forming agents[13,24] and higher agent loading[25] increases dope solution viscosity, reducing demixing rates during coagulation. This thickens the skin layer that reduces membrane permeability.

As industry seeks to become sustainable, the need to develop high performance membranes is as important as producing such membranes sustainably. Currently, dipolar aprotic solvents – DMF, NMP and DMAc are used to fabricate PES membranes. However, these solvents are categorized as "very high concern" by the European Chemicals Agency[26] and "undesired" by Pfizer's assessment.[27] The most straight-forward approach to fabricate polymer membranes sustainably is to replace DMF, NMP and DMAc with green solvents that provide similar properties and solubilities. This has been achieved using benign, bio-based solvents with strong polarity such as γ-valerolactone (GVL), dimethyl isosorbide (DMI) and dihydrolevoglucosenone (Cyrene™).[28] PES dope solutions prepared with γ-valerolactone yielded sponge-like membranes with no macrovoids after NIPS,[29] while replacing NMP with Cyrene™ typically yield membranes with dense structures and hence lower water fluxes after NIPS.[30,31] Alternatively, PES dope solutions prepared with dimethyl isosorbide can produce membranes with pure water permeance of 6300 L m^{-2} h^{-1} bar^{-1}.[32] However, this approach requires a complex coagulation process that combines VIPS and TIPS.

Here we hypothesize that the poor permeance of polymer membranes fabricated from benign solvents can be overcome with spray coating. Spray coating can reduce the thickness of polymeric selective layers in thin film composite membranes by 170-fold, from 53 μm to 0.3 μm, underpinning a 5-fold increase in pure water permeances.[33] This approach is also effective for depositing thin and smooth PDMS selective layers on PVDF membranes for biobutanol recovery.[34] The technique of spray coating has also been deployed to deposit active layers on porous membranes, such as a rough and porous cross-linked copolymer for oil/water separation,[35] and catalysts on inorganic support layers for a membrane electrode assembly.[36] These works focus mainly on depositing a selective or active layer on pre-formed porous membranes.

To validate our hypothesis, here we exploited spray coating to fabricate the porous support layers of TFC membranes to overcome the trade-off between the sustainability that Cyrene™ can offer in polymer membrane fabrication and poor separation performances. This was achieved by creating and encapsulating air bubbles within a wet polymer film to enhance demixing during NIPS, forming an atypical, sandwiched structure comprising a highly porous, ultra-thin skin layer and a sub-layer with finger-like pores interconnected with macrovoids located in the bottom layer (Scheme 1). This highly porous structure underpinned a pure water permeance of 68.9 L m^{-2} h^{-1} bar^{-1}, 7-fold higher than knife cast membranes from PES–Cyrene™ dope solutions. The deposition of a polyamide selective layer on spray-coated PES membranes yielded TFCs with water permeance of 1.76 L m^{-2} h^{-1} bar^{-1}. This was 480% and 110% higher than TFC membranes comprising knife cast PES support layers fabricated with Cyrene™ and NMP dope solutions, respectively. The increase in water permeance did not reduce NaCl rejection rate, indicating the feasibility of using spray coating to overcome the poor permeance of knife cast membranes produced using Cyrene™.
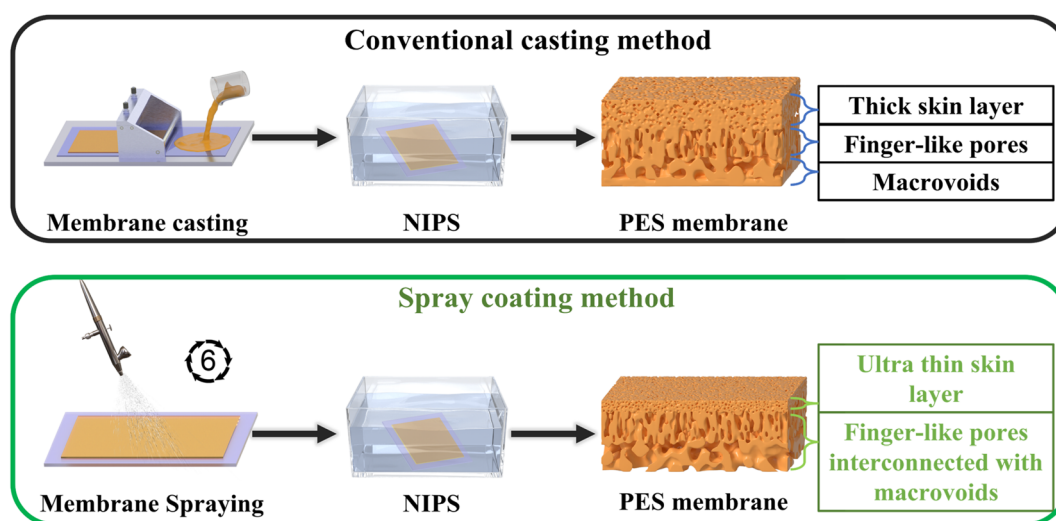
Scheme 1 Comparison of sandwich structure of PES membranes fabricated *via* the traditional method of knife casting (black box) and our proposed approach of automated spray coating (green box).

Experimental

Materials and equipment

Polyethersulfone (E3020) and Cyrene™ were purchased from Sigma Aldrich. Polyvinylpyrrolidone (PVP, K-30), m-phenyl-enediamine (MPD), 1-methyl-2-pyrrolidone (NMP), and 1,3,5-benzenetricarbonyl chloride (TMC, 98+%) were purchased from Alfa Aesar. N-Hexane was purchased from Acros Chemicals.

A Harder & Steenbeck Evolution CRplus Action Airbrush with a 0.6 mm nozzle set was purchased from Everything Airbrush, UK. A Creator Pro 3D printer was purchased from Flashforge, China. Servo motors, an Arduino Uno R3 board and connecting cables were purchased from RS Components Ltd, UK.

Modification of 3D printer into an automated spray coater

Manual spray coating of polymer solutions is difficult to replicate as parameters such as spraying speed, distance and angle must be consistent in between sprays. We overcome this limitation by automating spray coating with a 3D printer. This was achieved by modifying an off-the-shelf 3D printer (Flashforge Creator Pro) into an automated spray coater. A spray gun holder was designed using Autodesk Fusion 360 and fabricated via fused deposition modelling. The original dual printhead of the CreatorPro 3D printer was removed from the x–y axis moving tray, followed by the installation of the bespoke spray gun holder on the moving tray (Fig. S1†). Stepper motors driving the x–y axis tray were disconnected from the CreatorPro and reconnected to a control circuit (A4988 chip) which was controlled by an Arduino Uno R3 board. The Arduino was coded to enable and control movement in both stepper motors. Details of this modification and script can be found in the ESI.†

Conventional knife casting of PES porous support layers

PES dope solutions were prepared by dissolving 15 wt% PES and 0–5 wt% PVP i.e., porogen in Cyrene™ or NMP at 80 °C (see Table 1 for more details). These solutions were stirred magnetically until complete PES dissolution, forming viscous solutions that were degassed overnight. The PES dope solution was first cast on a glass plate using a casting knife (Elcometer 3700) set at a thickness of 200 μm and immersed immediately into a coagulation bath, forming a polymer membrane upon NIPS. Knife casting and NIPS were performed at room temperature. The PES membrane was left in the coagulation bath with the glass plate until it was detached completely from the glass. This free-standing PES membrane was then transferred into a water bath until further characterisation. Knife cast PES films were used here as control samples for benchmarking the performances of spray-coated membranes.

Spray coating PES porous support layers

Due to the toxicity of NMP, spray coating was only performed with PES dope solutions comprising Cyrene. PES dope solutions used in spray coating here were prepared using the same protocol mentioned above, except that the formulated dope solutions were used as is and not degassed. Upon dissolution of PES in Cyrene, this dope solution was loaded into the spray gun's solution reservoir. Spraying distance was set to 20 cm above a glass plate placed on the build plate of the 3D printer. The build plate was not heated prior and throughout spray coating. 4 bar of nitrogen was supplied to the spray gun and spray gun movement was controlled by the control circuit and stepper motors. The spray gun moved across the glass plate to ensure full coverage of the printing area. This process was repeated for 6 times at room temperature to produce a PES film with similar thickness (200 μm) to knife cast films. Details for this layer-by-layer polymer deposition are in the ESI (Fig. S2).† These spray-coated PES films were then subjected to the same NIPS protocol listed above.

Compared to knife casting, a key benefit of spray coating lies in reducing membrane fabrication time. With a casting speed of 3 cm s^{-1}, knife casting a 10 cm × 20 cm membrane is typically achieved within 10 s. Meanwhile, we took around 10 min to fabricate a PES film of similar size via spray coating. The key difference lies in how the dope solutions were prepared. Dope solutions for knife casting must be degassed for at least 2 hours to remove air bubbles that will otherwise create defective membranes. For spray coating, the dope solution was used as is, as air bubbles would inevitably be introduced into the solution during spray coating. This difference in dope solution preparation time underpins the reduction in time consumption associated with spray coating membranes.

Table 1 Composition of all dope solutions for fabricating PES membrane. K refers to knife cast PES and S refers to spray-coated PES

Fabricate method	Sample code	PES (wt%)	PVP (wt%)	Solvent (wt%)	
Knife casting	N-PES-K-0	15	0	NMP	85
	N-PES-K-1	15	1		84
	N-PES-K-3	15	3		82
	N-PES-K-5	15	5		80
	C-PES-K-0	15	0	Cyrene™	85
	C-PES-K-1	15	1		84
	C-PES-K-3	15	3		82
	C-PES-K-5	15	5		80
Spray coating	C-PES-S-0	15	0	Cyrene™	85
	C-PES-S-1	15	1		84
	C-PES-S-3	15	3		82
	C-PES-S-5	15	5		80

This journal is © The Royal Society of Chemistry 2023

J. Mater. Chem. A, 2023, **11**, 891–900 | **893**

All the resultant membranes and their corresponding dope compositions are listed in Table 1. The nomenclature for these membranes comprised information on the solvent type used in dope formulation, fabrication method and the amount of PVP porogens. For example, N-PES-K-0 referred to a PES membrane fabricated with NMP (N) as solvent and knife casting (K), with 0 wt% PVP. Likewise, C-PES-S-5 referred to a sample prepared using Cyrene™ (C) as solvent and spray coating (S), with 5 wt% PVP.

Fabrication of PA–PES TFC membranes

PES membranes fabricated from knife casting or spray coating were used as porous support layers for TFCs. A PES membrane was taped to a glass plate, with the top surface facing upwards and placed in an aqueous solution comprising 2 wt% MPD for 5 minutes. The amine-loaded PES support was removed from the solution and pressed with a roller to remove excess amine solution, prior immersion in a *n*-hexane solution comprising 0.2 wt% TMC for 2 min. The resultant TFC was placed in an oven at 50 °C for 5 min and washed with *n*-hexane and water to remove unreacted and residue MPD and TMC.

Scanning electron microscopy (SEM)

The skin layer and cross-section morphologies of membrane samples studied here were observed with a Carl Zeiss SIGMA HD VP Field Emission SEM. All samples were dried for 12 h in a vacuum oven before SEM analysis. For cross-section SEM characterization, membrane samples were first freeze-fractured in liquid nitrogen. A 10 nm-thin layer of gold was sputter-coated on to the samples before imaging. An accelerating voltage of 5 kV was used to obtain SEM micrographs.

Fourier transform infrared spectroscopy (FTIR)

FTIR was performed in attenuated total reflectance (ATR) mode on a Nicolet™ iS™ 20 FTIR Spectrometer (Thermo Scientific™) with a Smart iTX™ diamond accessory to characterise functional groups over a range of 500–4000 cm^{-1}. All samples were dried for 12 h in a vacuum oven before analysis. ATR-FTIR analyses (Fig. S3†) revealed that the use of Cyrene or spray coating did not alter the chemical structure of PES. The FTIR spectra of the top surface of C-PES-S-1 showed the characteristic bands of PES centred at 1104 cm^{-1} (C–O–C), 1148 cm^{-1} (S=O), 1240 cm^{-1} (C–O), 1320 cm^{-1} (C–SO$_2$–C), 1485 cm^{-1} and 1577 cm^{-1} (benzene ring).[37–39] After the deposition of the PA selective layer *via* interfacial polymerisation, three new peaks centred at 1538, 1609 and 1656 cm^{-1} were observed. These three peaks corresponded to C=O stretching (amide II bond), aromatic amide ring and N–H bending of amide I in –CO–NH– group, respectively.[40]

Water contact angle measurements

Water contact angles of membranes developed here were determined using an Ossila Contact Angle Goniometer using the sessile drop method. For each sample, three measurements

were performed, and averages and standard deviations were calculated.

Pure water permeance and salt rejection rate measurements

The pure water permeances of the PES and TFC membranes were measured using triplicate samples and a Sterlitech stainless steel HP4750 stirred dead-end cell. The feed solution comprised deionised water obtained from a lab-based water purification system and pressurised with nitrogen gas at 1 bar at room temperature to reach steady flow rate, then measured at 3 bars. During filtration, the feed solution was stirred at 400 rpm. Permeate samples were collected in capped flasks as a function of time, weighed, and analysed. The permeance was calculated using the following equation:

$$\text{Permeance} = \frac{V}{At\Delta P}$$

where permeance (L m^{-2} h^{-1} bar^{-1}) is expressed in terms of V, the volume of the solvent passing through the membrane (L), A – effective membrane area (m^2), t – operation time (h), and ΔP – the applied pressure (bar).

The salt rejection rates of TFC membranes were determined using a 2000 ppm NaCl water solution as feed solution and stirred at 400 rpm to avoid concentration polarization. The feed solution was pressurized at 3 bar to reach a steady flow rate and measured at 3 bar. The feed and permeate salt concentrations were measured by determine water conductivities with a SQ-7031 SciQuip salinity meter. Rejection rates of the TFC membranes were calculated using the following equation:

$$\text{Rejection rate} = \left(1 - \frac{C_p}{C_f}\right) \times 100$$

where C_p and C_f are the solute concentrations in the permeate and feed solution, respectively.

Zeta-potential measurement

The surface potential of membranes studied here was characterized by streaming potential method using an AgCl electrode analyser (SurPASS™^{3}, AntonParr, Austria). 1 cm × 2 cm membranes were fixed on a double stack mould, so that the surface charge of the barrier layer could be analysed. A solution of 0.001 M KCl (aq.) was utilized to provide the background ionic strength, and automatic titration was performed using 0.1 M HCl (aq.) and 0.1 M NaOH (aq.) to investigate the effect of pH (3 to 10) on zeta-potential.

Atomic force microscopy

AFM topography images of the PES supports were obtained using a Nanoscope IIIa Multimode scanning probe microscope (Bruker AXS Inc) with an E-scanner in tapping mode using silicon cantilevers. No other image processing was applied except flattening, which was performed here using Gwyddion.
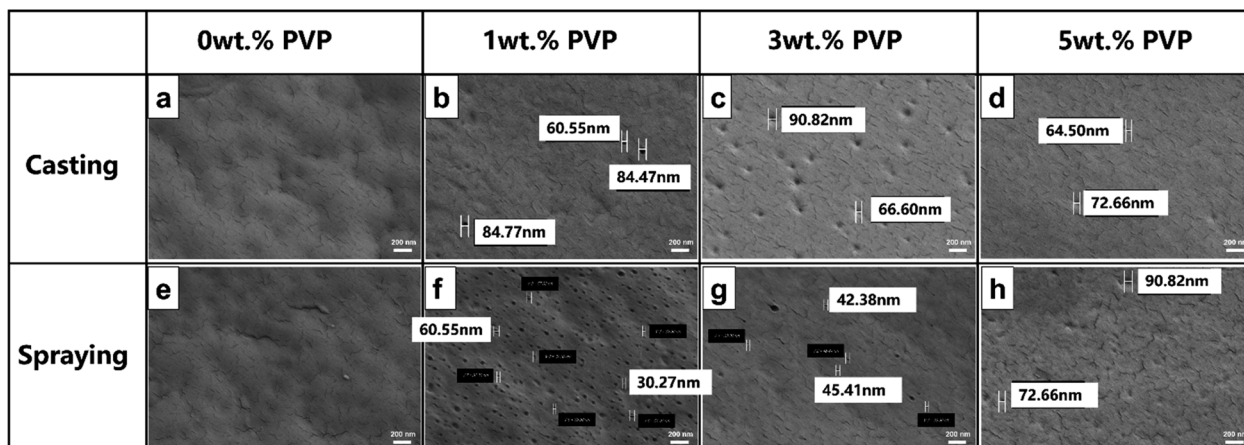
894 | *J. Mater. Chem. A*, 2023, **11**, 891–900

This journal is © The Royal Society of Chemistry 2023

Fig. 1 SEM micrographs of (a–d) knife cast and (e–h) spray-coated PES membranes from Cyrene dope solutions with PVP loading from 0, 1, 3 and 5 wt% showed that spray coating generated more and smaller pores in PES membrane surfaces.

Results and discussion

Film morphology and structure

The top surfaces of spray-coated PES membranes fabricated from Cyrene-based dope solutions were more porous than those from knife casting as PVP content increased from 0 to 5 wt% (Fig. 1). Regardless of fabrication method, without pore forming agents, in this case, PVP, the top surfaces of PES membranes were non-porous (Fig. 1a and e). PES films fabricated from Cyrene-based dope solutions containing 1 wt% PVP yielded the most porous top surface. On average, the sizes of these pores were less than 100 nm. Spray coating generated more and smaller pores in PES membranes (Fig. 1b and f). As PVP loading increased to 3 and 5 wt%, the top surfaces of PES membranes were smoothened, closing top surface pores. The effect of PVP content on PES surface porosity was also observed in knife cast membranes using NMP-based dope solutions (Fig. S6 and S7†). AFM analyses showed that the top surface morphologies of PES membranes fabricated from NMP-based dope solutions were smoother than those from Cyrene (Fig. 2). The surface roughness (R_q) value of N-PES-K-1 membrane was 11.3 ± 3.21 nm, attributing to a ridge-and-valley structure. By replacing NMP with Cyrene, the R_q of C-PES-K-1 increased by 166%, reaching 30.1 ± 5.11 nm. Spray coating did not significantly alter the R_q value of C-PES-S-1, reaching a value of 31.95 ± 4.76 nm. The surface pores of C-PES-S-1 could be clearly observed, but not for C-PES-K-1 and N-PES-K-1. This may be due to the different immiscibility of Cyrene/water and NMP/water. Cyrene is more miscible with water than NMP. This leads to slower and non-uniform precipitation across the dope solution film.[30] This could increase surface porosity and surface roughness surface, which was also in line with the trends in surface morphologies shown in Fig. 1.

Other than surface roughness and porosity, using Cyrene in PES membrane fabrication also altered skin thickness and sub-layer structure (Fig. 3, S8 and S9†). The structures of all PES membranes studied here, regardless of solvents (Cyrene or NMP) used in dope solution or fabrication approach (spray

coating or knife casting), were asymmetric, consisting of a skin layer on top and a porous sub-layer with finger-like pores and macro voids. Meanwhile, an additional bottom porous layer was
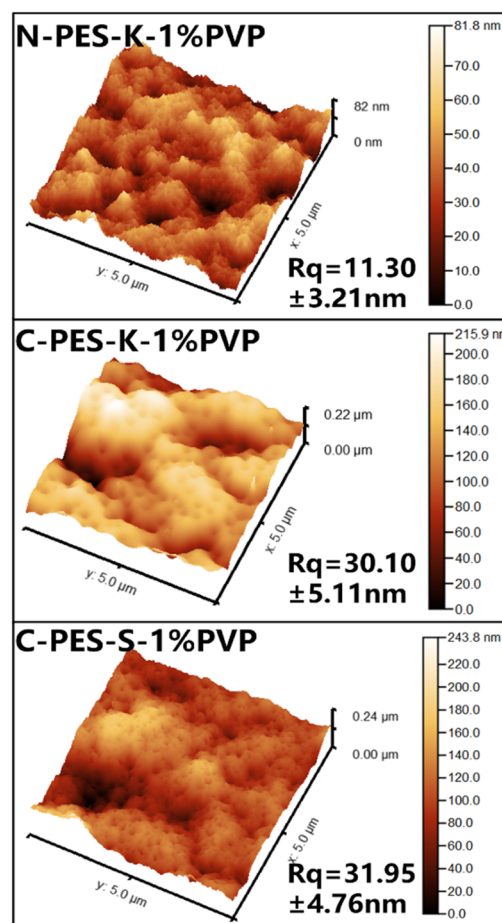

Fig. 2 AFM images and corresponding surface roughness of PES membranes fabricated by knife casting (top) an NMP- and (middle) Cyrene-based dope solution, and (bottom) spray coating a Cyrene-based dope solution. These dope solutions contain 1 wt% PVP.
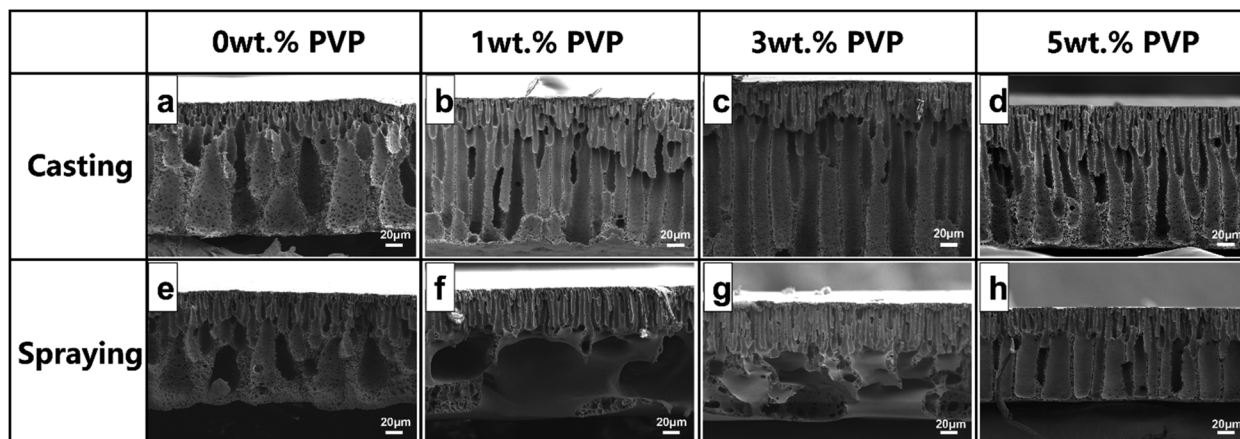
Fig. 3 SEM micrographs of cross-sections of (a–d) knife cast and (e–h) spray-coated PES membranes from Cyrene dope solutions with PVP loading from 0, 1, 3 and 5 wt% showed that spray coating creates more porous PES membranes than the conventional method of knife casting.

observed across all knife cast membranes. The asymmetric structures of knife cast membranes (N-PES-K and C-PES-K) comprised of macro voids that began to merge into larger voids when PVP was added into the dope solution. We also observed that there were less sponge-like structures as the macro voids merged. As PVP loading increased from 0 to 5 wt%, the finger-like pores became more dominant in all samples. This indicated that PVP was an excellent pore-forming additive. There were more interconnected pores within the finger-like channel walls in membranes prepared from Cyrene™. This was also observed in the work of McElroy and co-workers.[31]

Compared to PES membranes fabricated with NMP (Fig. S7†), the finger-like channels in membranes produced using Cyrene™ were more vertical and well-structured. The cross-sections of C-PES-K-0 and C-PES-S-0 were similar where finger-like pores and macro voids were observed below the skin layer. The macro voids in C-PES-S-0 were interconnected with pores. These interconnected pores could reduce the hydraulic resistance and enhance membrane permeability.[41] We did not observe large macro voids in the sub-layer of knife cast membranes fabricated with Cyrene, even with the ideal PVP loading of 1 wt%. Macro voids below the finger-like pores were only observed in spray-coated membranes fabricated with Cyrene-based dope solutions comprising 1 wt% and 3 wt% PVP (C-PES-S-1 and C-PES-S-3). The finger-like pores and macro voids merged into an ultra-porous sub-layer. Hence, the asymmetric structures of spray-coated membranes comprised of only two layers – an ultra-thin and porous skin layer and an ultra-porous sub-layer made up of interconnected finger-like macro voids. This dual layer asymmetric structure was unique to spray-coated membranes as a distinctive third bottom layer was observed across all knife cast membranes studied here. We also observed that there were less polymer structures within the macro voids of C-PES-K-1 and C-PES-S-1 samples. This lack of polymer structures could be beneficial for enhancing permeability. However, with 5 wt% PVP, the macro voids of C-PES-S-5 became less obvious as they merged with finger-like pores.

Apart from sub-layer structural changes, we also observed that the skin layer thicknesses varied as a function of solvent type and fabrication approach (Fig. S8 and S9†). As PVP content increased from 0 to 5 wt%, the thicknesses of skin layers of knife cast PES membranes produced with Cyrene (C-PES-K) and NMP (N-PES-K) increased from 348 nm to 1352 nm and 464 nm to 1312 nm, respectively. Thick skin layers are known to reduce permeabilities of PES membranes.[31,42] The formation of thick skin layers in knife cast membranes could be explained from the perspective of mass transfer.[43,44]

Membrane formation from knife cast dope solutions typically occur over two phases:[43,44] (1) solvent exchange during initial contact between the working solvent in the cast polymer dope film (NMP) and the non-solvent in the coagulation bath (water) while there is no movement between PES and PVP, and (2) after the initial contact phase, water molecules penetrated further into the cast solution. This enabled PES–PVP diffusion and demixing as PVP is a water-soluble pore forming polymeric additive, while PES is immiscible with water. The duration of solvent exchange was mainly governed by the additive's hydrophilicity and the thermodynamic stability of the PES–NMP–PVP system. Given the short time scale of the initial phase, varying additive content would not affect this duration significantly. However, higher additive content enhanced hydrophilicity of PES–PVP mixtures and hence increasing initial solvent exchange rate where rapid leaching of PES–PVP mixtures led to the formation of dense and thick skin layers. Calculations from Boom *et al.* showed that the non-solvent fluxes through the interface increased nearly 3 times as the membrane forming porogen/polymer ratio increased from 0 to 0.25.[43] Here, our PVP/PES ratio reached 0.067. Fang *et al.* also reported similar skin layer thickening effects when varying the loading of pore forming agents in PES membrane fabrication.[25]

The formation of thick skin layers in PES membranes was overcome here with spray coating. The skin layers of spray-coated membranes were less than 100 nm thin, 6× thinner than those from knife casting (Fig. S9†). Using a gas pressure to

enable spray coating, polymer droplets separated by air bubbles were deposited non-uniformly on to substrates, forming a rough surface comprising loosely connected island-like structure (Fig. S4†). As more polymer droplets were deposited on top of the initial layer in subsequent spray runs, these air bubbles were encapsulated and remained intact (Fig. S5†). Subsequent deposition of more polymer droplets formed a smooth-looking structure. These encapsulated air bubbles were key to forming porous films whilst enabling instantaneous demixing – the pre-requisite for the formation of ultra-thin skin layers. The average diameters of these air bubbles were less than 0.1 to 0.15 μm (Fig. S5b†), matching the macro-voids shown in (Fig. 3f). As observed in all spray-coated samples, after a skin layer was formed, the number of macro voids with thick walls decreased with the addition of PVP and were replaced with interconnected vertical finger-like pores with thinner walls. This was due to the faster non-solvent penetration from the skin layer to sub-layer, which was in line with the abovementioned skin layer thickening effect: higher PVP content enhanced solvent and non-solvent exchange rates that consequently thickened the skin layer, but at the same time, non-solvent (water) also reached the sub-layer faster, which then suppressed macro void formation.[25,44]

Water contact angle, zeta-potential, and permeances of all prepared PES membrane

The addition of PVP into PES dope solutions altered the hydrophilicity of resultant membranes (Fig. 4a). Lower values of water contact angle indicated more hydrophilic surfaces.[45] Here we observed that regardless of solvents used in the dope solution and film formation method, the increase in PVP content from 0 to 5 wt% reduced the water contact angles of PES membranes studied here in the following order: N-PES-K > C-PES-K > C-PES-S. Membranes prepared using Cyrene typically show lower water contact angles i.e., more hydrophilic.[46,47] This trend was identical to the surface porosity of these membranes and inverse of surface roughness. Membranes with porous surface reduced the water contact angle as water droplets spread out faster.[48]

The surfaces of spray-coated PES membranes were the roughest amongst all membranes studied here, hence their surfaces were the most negatively charged across a pH range of 3 to 9 (Fig. 4b). Increased surface roughness enhances surface charge density i.e. rough surfaces tend to more negatively charged.[46] Surface charges of membranes are a critical parameter for separations, especially for salt rejection. All PES membranes studied here were negatively charged at pH around 4.[46,49,50] Among all the PES membrane samples, C-PES-S demonstrated the most negative zeta potential value. This was in line with their surface morphologies shown in SEM micrographs and their surface roughness values in AFM analyses. The hydrophilicity, surface porosity and surface roughness[51,52] were key reasons why spray-coated membranes were more permeable than knife cast membranes.

PES membranes fabricated from spray coating were more permeable than knife cast membranes (Fig. 4c). The pure water
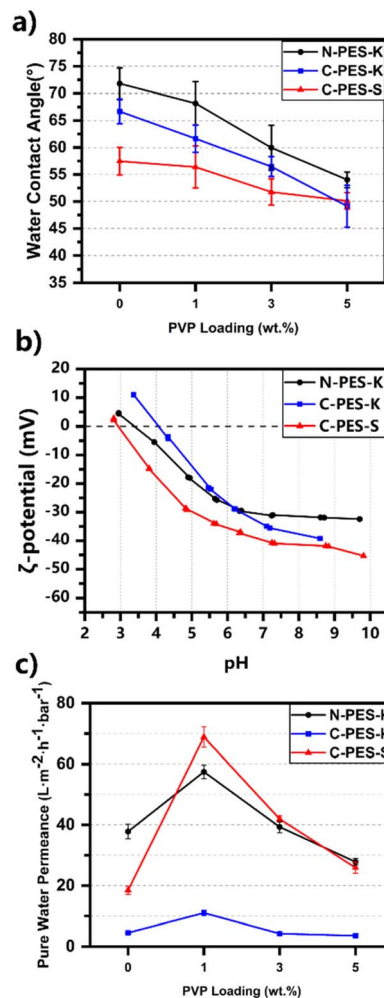

Fig. 4 (a) Water contact angles, (b) zeta-potential, and (c) pure water permeances of PES membranes fabricated by knife casting with NMP- (black) and Cyrene- (blue) based dope solutions and spray coating (red).

permeances of PES membranes increased as PVP content increased from 0 to 1 wt% and decreased with 3 and 5 wt% PVP content. This was attributed to the contrasting effects of hydrophilicity, porosity improvements and skin layer thickening. Amongst all membranes studied here, spray-coated membranes fabricated with Cyrene-based dope solutions containing 1 wt% PVP, were the most permeable, with a pure water permeance of 68.867 L m^{-2} h^{-1} bar^{-1}. Meanwhile the pure water permeance of the most permeable knife cast PES membrane fabricated in this work only reached 11.033 L m^{-2} h^{-1} bar^{-1}, like those reported in literature.[31,42] This was 6-fold lower than spray-coated membranes and those of PES membranes fabricated by NMP and DMAc (Table 2). The only difference between these two membrane types lies in the way they were fabricated – spray coating vs. knife casting. This difference in membrane fabrication highlighted how spray coating could yield membranes with an ultra-thin, porous skin layer and sub-layer comprising finger-like pores interconnected with macro voids to overcome the limitations of using benign,

Table 2 Comparison of fluxes and permeances of PES membranes fabricated by different types of solvent

Membrane flux ($L\ m^{-2}\ h^{-1}$)	Pressure (bar)	Permeance ($L\ m^{-2}\ h^{-1}\ bar^{-1}$)	Solvent type	Ref.
8.2	6	1.367	DMAc	53
9.3	4	2.325	DMAc	54
14.69	3	4.897	DMAc	55
133.29	3	44.43	DMAc	56
31.8	5	6.36	NMP	57
39.4	1	39.4	NMP	58
<80	2	<40	NMP	59
49.4	1	49.4	NMP	60
10.512	5	2.102	Cyrene™	31
206.6	3	68.867	Cyrene™	This work

biobased solvents for polymer membrane fabrication. Compared to a typical N-PES-K membrane, spray coating improved pure water permeance by 20%.

Fig. 5 (a) Zeta-potential, (b) permeance, and (c) NaCl rejection rates of TFC membranes comprising a PA selective layer deposited on PES membranes fabricated from knife casting NMP (black) and Cyrene (blue) dope solutions, and spray coating (red) Cyrene-based dope solutions containing 1 wt% PVP. The TFC permeance and NaCl rejection rates were determined using a dead end cell at 3 bar and a 2000 ppm NaCl aqueous solution.

The effect of spray coating on membrane mechanical properties and water permeance stability were also evaluated (Fig. S10 and Table S1†). The tensile stress at break had an order of C-PES-K > N-PES-K > C-PES-S, ranging from 2.619 MPa to 2.096 MPa, which was the result of skin layer thickness and sublayer macrovoids.[61,62] This indicated that spray coating method reduced the skin layer thickness without drastically sacrificing mechanical properties. Further cyclic water filtration test also proved that membranes produced by spray coating were mechanically stable after 5 repeated 1 hour tests at 3 bar. Clearly, spray coating is feasible for fabricating PES membranes in a sustainable way by enabling the replacement of NMP with Cyrene whilst delivering more permeable membranes.

Desalination performances of TFC membranes

To further demonstrate the application of spray-coated PES films, we deployed these membranes as the porous supports of TFCs. We deposited thin PA selective layers on the top surfaces of spray-coated PES films (Fig. S11†). This was achieved through interfacial polymerisation of MPD and TMC, following well-established protocols.[63] This PA selective layer reduced the zeta-potential values of resultant membranes (Fig. 5a). These were more negative than pristine spray-coated PES membranes *i.e.*, a higher surface charge density which could enhance salt rejection. As such, PA/C-PES-S-1 TFC presented the highest permeance of 1.76 $L\ m^{-2}\ h^{-1}\ bar^{-1}$ among all samples studied here for a 2000 ppm NaCl solution, with 92.4% salt rejection rates (Fig. 5b and c), amongst all membranes studied here. The salt rejection rates of TFC membranes comprising spray-coated PES support layers were like those comprising conventional knife cast support layers.[63,64]

Conclusion

In this study, we show that automated spray coating could be used to fabricate high performance PES membranes in a sustainable manner. The key benefit of using spray coating to fabricate membranes lies in producing membranes with a rough, ultra-thin, porous skin layer and ultra-porous sub-layer consisting of finger-like pores interconnected with macro voids *i.e.*, an open-ended porous bottom layer. A comparison between the water permeances of spray-coated and knife cast PES
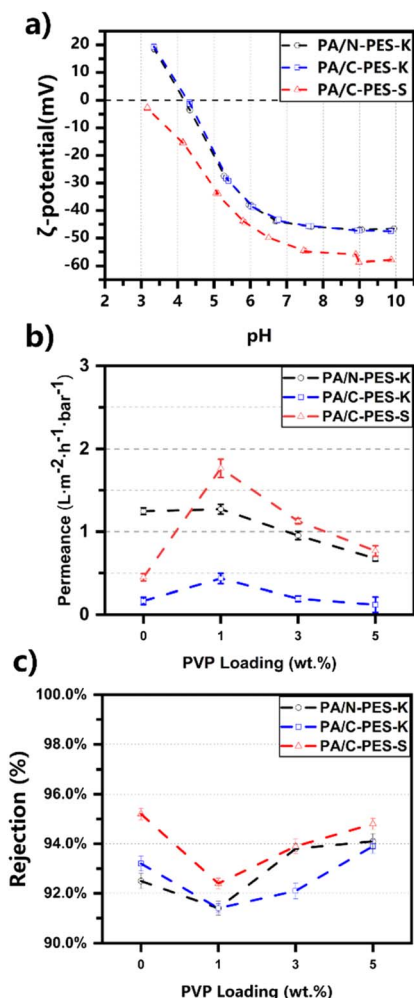
898 | *J. Mater. Chem. A*, 2023, **11**, 891–900

This journal is © The Royal Society of Chemistry 2023

membranes showed that spray coating can overcome the trade-off between lower separation performances and sustainability in membrane fabrication by replacing hazardous solvents like NMP with benign solvents like Cyrene™. This work has successfully resolved this conundrum and showed that automated spray coating could potentially pave the way towards scalable, sustainable membrane fabrication.

Conflicts of interest

There are no conflicts to declare.

Acknowledgements

References

1 S. Bandehali, A. E. Amooghin, H. Sanaeepur, R. Ahmadi, A. Fuoco, J. C. Jansen and S. Shirazian, *Sep. Purif. Technol.*, 2021, **278**, 119513–119558.

2 S. Luo, Q. Zhang, L. Zhu, H. Lin, B. A. Kazanowska, C. M. Doherty, A. J. Hill, P. Gao and R. Guo, *Chem. Mater.*, 2018, **30**, 5322–5332.

3 G. Liu, W. Wei, W. Jin and N. Xu, *Chin. J. Chem. Eng.*, 2012, **20**, 62–70.

4 A. G. Fane, R. Wang and M. X. Hu, *Angew. Chem., Int. Ed. Engl.*, 2015, **54**, 3368–3386.

5 Y. Liao, C.-H. Loh, M. Tian, R. Wang and A. G. Fane, *Prog. Polym. Sci.*, 2018, **77**, 69–94.

6 J. Hu, Y. Chen, J. Lu, X. Fan, J. Li, Z. Li, G. Zeng and W. Liu, *Polymer*, 2020, **201**, 122531–122541.

7 Z. Chu, K. Chen, C. Xiao, H. Ling and Z. Hu, *Polymer*, 2020, **188**, 122160–122170.

8 Z.-L. Xu and F. A. Qusay, *J. Membr. Sci.*, 2004, **233**, 101–111.

9 C. Zhao, J. Xue, F. Ran and S. Sun, *Prog. Mater. Sci.*, 2013, **58**, 76–150.

10 H. H. Wang, J. T. Jung, J. F. Kim, S. Kim, E. Drioli and Y. M. Lee, *J. Membr. Sci.*, 2019, **574**, 44–54.

11 C. Alexowsky, M. Bojarska and M. Ulbricht, *J. Membr. Sci.*, 2019, **577**, 69–78.

12 J. F. Kim, J. H. Kim, Y. M. Lee and E. Drioli, *AIChE J.*, 2016, **62**, 461–490.

13 M. Khorsand-Ghayeni, J. Barzin, M. Zandi and M. Kowsari, *Polym. Bull.*, 2017, **74**, 2081–2097.

14 M. A. A. Shahmirzadi, S. S. Hosseini, G. Ruan and N. R. Tan, *RSC Adv.*, 2015, **5**, 49080–49097.

15 S. Madaeni and A. Taheri, *J. Polym. Eng.*, 2009, **29**, 183–198.

16 J. He, A. Cui, F. Ni, S. Deng, F. Shen, C. Song, L. Lou, D. Tian, C. Huang and L. Long, *J. Colloid Interface Sci.*, 2019, **536**, 710–721.

17 J. He, D. Xiong, P. Zhou, X. Xiao, F. Ni, S. Deng, F. Shen, D. Tian, L. Long and L. Luo, *Chem. Eng. J.*, 2020, **393**, 124696.

18 M. R. Cervellere, X. Qian, D. M. Ford, C. Carbrello, S. Giglia and P. C. Millett, *J. Membr. Sci.*, 2021, **619**, 118779.

19 A. Bildyukevich, T. Hliavitskaya, S. Pratsenko and G. Melnikova, *Membr. Membr. Technol.*, 2021, **3**, 24–35.

20 M. Esmaeili, J. Lahti, T. Virtanen, M. Mänttäri and M. Kallioinen, *Sep. Purif. Technol.*, 2020, **235**, 116225.

21 C.-C. Ho, J. F. Su and L.-P. Cheng, *Polymer*, 2021, **217**, 123451.

22 S. Vidya, A. Vijayalakshmi, A. Nagendran and D. Mohan, *Sep. Sci. Technol.*, 2008, **43**, 1933–1954.

23 D.-y. Zuo, Y.-y. Xu, W.-l. Xu and H.-t. Zou, *Chin. J. Polym. Sci.*, 2008, **26**, 405–414.

24 Y. Mansourpanah, A. Gheshlaghi and F. Rekabdar, *Desalin. Water Treat.*, 2012, **50**, 302–309.

25 X. Fang, J. Li, X. Li, X. Sun, J. Shen, W. Han and L. Wang, *J. Membr. Sci.*, 2015, **476**, 216–223.

26 J. Esteban, A. J. Vorholt and W. Leitner, *Green Chem.*, 2020, **22**, 2097–2128.

27 K. Alfonsi, J. Colberg, P. J. Dunn, T. Fevig, S. Jennings, T. A. Johnson, H. P. Kleine, C. Knight, M. A. Nagy and D. A. Perry, *Green Chem.*, 2008, **10**, 31–36.

28 F. Gao, R. Bai, F. Ferlin, L. Vaccaro, M. Li and Y. Gu, *Green Chem.*, 2020, **22**, 6240–6257.

29 M. A. Rasool and I. F. Vankelecom, *Membranes*, 2021, **11**, 418.

30 S. Mohsenpour, S. Leaper, J. Shokri, M. Alberto and P. Gorgojo, *J. Membr. Sci.*, 2022, **641**, 119924–119939.

31 R. A. Milescu, A. Zhenova, M. Vastano, R. Gammons, S. Lin, C. H. Lau, J. H. Clark, C. R. McElroy and A. Pellis, *ChemSusChem*, 2021, **14**, 3367–3381.

32 F. Russo, F. Galiano, F. Pedace, F. Aricò and A. Figoli, *ACS Sustainable Chem. Eng.*, 2019, **8**, 659–668.

33 Y. L. Xue, J. Huang, C. H. Lau, B. Cao and P. Li, *Nat. Commun.*, 2020, **11**, 1461.

34 C. Cheng, D. Yang, M. Bao and C. Xue, *J. Appl. Polym. Sci.*, 2020, **138**, 49738–49748.

35 J. Xing, G. Zhang, X. Jia, D. Liu and I. Wyman, *ACS Appl. Mater. Interfaces*, 2021, **13**, 4485–4498.

36 M. Klingele, B. Britton, M. Breitwieser, S. Vierrath, R. Zengerle, S. Holdcroft and S. Thiele, *Electrochem. Commun.*, 2016, **70**, 65–68.

37 C.-C. Ho, J. F. Su and L.-P. Cheng, *Polymer*, 2021, **217**, 123451.

38 M. J. Luján-Facundo, J. A. Mendoza-Roca, B. Cuartas-Uribe and S. Álvarez-Blanco, *J. Food Eng.*, 2015, **163**, 1–8.

39 R. A. Milescu, C. R. McElroy, T. J. Farmer, P. M. Williams, M. J. Walters and J. H. Clark, *Adv. Polym. Technol.*, 2019, **2019**, 1–15.

40 B. Khorshidi, T. Thundat, B. A. Fleck and M. Sadrzadeh, *RSC Adv.*, 2015, **5**, 54985–54997.

41 C. C. Ho and A. L. Zydney, *J. Membr. Sci.*, 1999, **155**, 261–275.

42 T. Marino, F. Galiano, A. Molino and A. Figoli, *J. Membr. Sci.*, 2019, **580**, 224–234.

43 R. Boom, T. Van den Boomgaard and C. Smolders, *J. Membr. Sci.*, 1994, **90**, 231–249.

44 J.-H. Kim and K.-H. Lee, *J. Membr. Sci.*, 1998, **138**, 153–163.

This journal is © The Royal Society of Chemistry 2023

J. Mater. Chem. A, 2023, **11**, 891–900 | **899**

45 A. L. Ahmad, A. A. Abdulkarim, B. S. Ooi and S. Ismail, *Chem. Eng. J.*, 2013, **223**, 246–267.

46 S. Ghiasi, A. Behboudi, T. Mohammadi and S. Khanlari, *Colloids Surf., A*, 2019, **580**, 123753–123767.

47 N. H. Ismail, W. N. W. Salleh, A. F. Ismail, H. Hasbullah, N. Yusof, F. Aziz and J. Jaafar, *Sep. Purif. Technol.*, 2020, **233**, 18.

48 S. Krainer and U. Hirn, *Colloids Surf., A*, 2021, **619**, 126503–126512.

49 A. F. Ismail and A. R. Hassan, *Sep. Purif. Technol.*, 2007, **55**, 98–109.

50 J. Chen, Z. Li, C. Wang, H. Wu and G. Liu, *RSC Adv.*, 2016, **6**, 112148–112157.

51 C.-C. Chang, S.-T. Yu, J. F. Su and L.-P. Cheng, *J. Polym. Res.*, 2022, **29**, 23.

52 W. Shao, S. Wu, Z. Hong, Q. Wang, Y. Xiong, R. Yi, Q. Xie and Z. Xiao, *J. Appl. Polym. Sci.*, 2016, **133**, 43769–43776.

53 S. Zinadini, A. A. Zinatizadeh, M. Rahimi, V. Vatanpour and H. Zangeneh, *J. Membr. Sci.*, 2014, **453**, 292–301.

54 S. Zinadini, A. A. L. Zinatizadeh, M. Rahimi and V. Vatanpour, *J. Ind. Eng. Chem.*, 2017, **46**, 9–18.

55 F. Mohammadnezhad, M. Feyzi and S. Zinadini, *J. Ind. Eng. Chem.*, 2019, **71**, 99–111.

56 F. Gholami, S. Zinadini, A. A. Zinatizadeh and A. R. Abbasi, *Sep. Purif. Technol.*, 2018, **194**, 272–280.

57 T. Tavangar, M. Karimi, M. Rezakazemi, K. R. Reddy and T. M. Aminabhavi, *Chem. Eng. J.*, 2020, **385**, 123787–123800.

58 R. J. Gohari, W. J. Lau, T. Matsuura and A. F. Ismail, *Sep. Purif. Technol.*, 2013, **118**, 64–72.

59 S. Zhang, P. Sukitpaneenit and T.-S. Chung, *Chem. Eng. J.*, 2014, **241**, 457–465.

60 L. Shen, X. Bian, X. Lu, L. Shi, Z. Liu, L. Chen, Z. Hou and K. Fan, *Desalination*, 2012, **293**, 21–29.

61 G. Arthanareeswaran and V. M. Starov, *Desalination*, 2011, **267**, 57–63.

62 S. A. Al Malek, M. N. Abu Seman, D. Johnson and N. Hilal, *Desalination*, 2012, **288**, 31–39.

63 A. P. Rao, S. Joshi, J. Trivedi, C. Devmurari and V. Shah, *J. Membr. Sci.*, 2003, **211**, 13–24.

64 X. Wei, Z. Wang, J. Chen, J. Wang and S. Wang, *J. Membr. Sci.*, 2010, **346**, 152–162.